Structured interference optical coherence tomography

Ji Yi*, Qing Wei, Hao F. Zhang and Vadim Backman

Department of Biomedical Engineering, Northwestern University, 2145 Sheridan Rd., Evanston 60208, USA

** Corresponding author: ji-yi@northwestern.edu*

Compiled May 24, 2012

We developed a structured interference optical coherence tomography (SIOCT) to enhance the lateral resolution beyond the diffraction limit. A sinusoidal pattern is created on the interferometric beam with the reference intensity temporally modulated. In the Fourier domain, the high spatial frequencies are shifted into the detectable range which therefore enhances the lateral resolution beyond the diffraction limit by a factor of two. The lateral resolution of SIOCT was characterized in our study as $\sim 5.5\mu m$ surpassing the diffraction limit $\sim 9.6\mu m$ as in conventional Fourier-domain OCT (FDOCT). SIOCT was demonstrated on phantoms and *ex vivo* adipose tissues.

OCIS codes: 170.4500, 100.6640.

Optical coherence tomography (OCT) is a 3D imaging modality with micron-level resolution and millimeter-level penetration depth [1,2]. The illumination on a typical OCT system is implemented by a confocal scheme that allows a focused Gaussian beam to scan laterally. The full-width-half-maximum (FWHM) and the Rayleigh range of the beam determines the lateral resolution and the depth of focus, which pose an inherent trade-off. By using an objective lens with higher numerical aperture, the resolution can be increased but the depth of focus will be shortened. To overcome this limitation, different approaches have been developed. One approach is to numerically solve the scattering problem that recovers the resolution out of the Rayleigh range without other additional hardware [3,4]. The other approach is to modify the beam profile that extends the depth of focus while maintaining the resolution, for example, to create the Bessel beam illumination [5–9]. With those improvements, however, the lateral resolution is still constrained by the diffraction limit.

Here we present a technique to enhance the lateral resolution beyond the diffraction limit by structured interference in OCT, while the depth of focus is kept the same. The idea comes from structured illumination which has been demonstrated with wide field illumination with the image of a periodic grating projected on the subject [10]. The high spatial frequency components of the sample together with the illumination pattern produces moiré fringes. In the Fourier space, the delta function resulted from the periodic pattern shifts the high spatial frequencies into the detectable range. With the extended spatial frequency, the resolution is ultimately enhanced by two-fold beyond the diffraction limit. Alternatively, the structured illumination can be realized in the confocal scheme with a scanning beam [11]. As Fig. 1(a) shows, when the focal spot is linearly steered along the lateral direction, the temporally modulated intensity is transformed to a spatial pattern to the same effect as in the wide field structured illumination. Typically the incident intensity on the sample needs to be modulated, while in OCT it can be the reference intensity that is modulated due to the interferometric principle.

With the structured interference, the B-scan image in SIOCT can be approximated as

$$I(x,z) = I_0 R(x,z)[1 + m\cos(k_m x + \phi_0)], |m| \leq 1 \quad (1)$$

where x and z denotes the lateral and axial positions; I and R denotes the image intensity and the true reflectance of tissue with I_0 being the incident intensity; m, k_m and ϕ_0 denote the amplitude, frequency and the initial phase of the modulation pattern. In SIOCT, the structured interference is on the lateral extent, which is independent of the axial profile obtained by an inverse Fourier transform (IFT) of the interference spectrum. Thus we will omit the parameter z from this point on. The spatial frequency distribution is the Fourier transform (FT) of the image intensity,

$$\begin{aligned}\tilde{I}(k_x)/I_0 =& \tilde{R}(k_x) + \frac{m}{2}e^{j\phi_0}\tilde{R}(k_x - k_m) \\ &+ \frac{m}{2}e^{-j\phi_0}\tilde{R}(k_x + k_m),\end{aligned} \quad (2)$$

where $\tilde{I}$ denotes the FT of I. We will use the tilde symbol to represent the FT throughout this paper. k_x denotes the spatial frequency along the x direction. The optical transport function (OTF) of the system plays an equivalent role as a low pass filter in the spatial frequency domain and the cut-off k_x determines the diffraction limited resolution. After shifting the k_x distribution by the structured interference as the last two terms in the above equation, high spatial frequencies can be shifted into the range of OTF and detected. In principle, the range of OTF is increased by twice when k_m is equal to the cut-off frequency of initial OTF, and thus the resolution is enhanced by a factor of two beyond the diffraction limit. In order to separate three terms in Equ. 2, several frames of B-scan images are required with the interference pattern shifted. Assuming that the phase shift of the pattern

between consequential frames is constant, Equ. 2 can be rewritten as

$$\tilde{I}(k_x,n)/I_0 = \tilde{R}(k_x) + \frac{m}{2}e^{j(n\Delta\phi+\phi_0)}\tilde{R}(k_x-k_m) + \frac{m}{2}e^{-j(n\Delta\phi+\phi_0)}\tilde{R}(k_x+k_m), \quad (3)$$

where $\Delta\phi$ denotes the constant phase shift of the interference pattern between frames and $n = 0, 1, 2...$ denotes the frame number. By another FT in terms of the frame number n, the second and the third term can be separated completely from the first term:

$$\tilde{\tilde{I}}(k_x,k_n)/I_0 = \tilde{R}(k_x)\delta(k_n) + \frac{m}{2}e^{j\phi_0}\delta(k_n-\Delta\phi)\times \tilde{R}(k_x-k_m) + \frac{m}{2}e^{-j\phi_0}\delta(k_n+\Delta\phi)\tilde{R}(k_x+k_m), \quad (4)$$

where k_n and n are Fourier pairs, and the *delta* functions separate the three terms in the k_n space. The extended spatial frequency can then be shifted to the reciprocal space of the original $\tilde{R}(k_x)$.

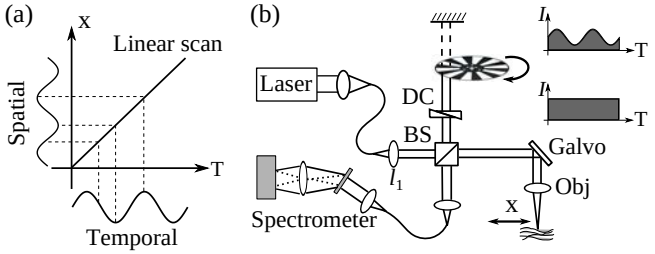

Fig. 1. (a) Under a raster linear scan, the temporal modulation is transformed into a spatial illumination pattern. The frequency of the temporal modulation determines the period of the pattern. (b) A cube beamsplitter (BS) forms a open space Michelson interferometer. The reference arm contained a dispersion control (DC), a mirror and an optical chopper for temporal intensity modulation.

Experimentally, a conventional Fourier-domain OCT system is adapted and an optical chopper is installed on the path of the reference arm (Fig. 1b). The illumination comes from a supercontinuum source (SuperK, NKT) with bandwidth from 650-800nm, yielding the axial resolution of $\sim 1.5\mu m$ in air. A Gaussian focus beam creates the illumination and is steered by the galvo mirror. The theoretical FWHM is $\sim 9\mu m$ in air (single mode field diameter: $4.6\mu m$@680nm, l_1: $f = 10mm$, Obj: $f = 33mm$). Each B-scan is composed of 256 A-lines (2.56kHz A-scan rate). The B-scan rate is 10 fps and the period of the illumination pattern is configured to be 12 μm. The sampling interval between adjacent A-lines depends on the scanning range. With $250\mu m$ scanning range, the A-line interval is $\sim 1\mu m$. The number of the modulation periods during one B-scan is non-integer so that the subsequent B-scan can have slight phase shifts of the pattern as the $\Delta\phi$ in Equ. 2. For a better SNR, ten frames were acquired with the total phase shift equal to 2π.

During the data processing, two FT are first performed on x and n according to Equ. 4 to separate the three spatial frequency terms. Secondly, these three terms are multiplied by a top head window with the width of the OTF of the system, then normalized by the OTF which is a Gaussian form whose width is determined by the system resolution. Next, the two shifted spatial frequency terms are shifted back by $\pm k_m$. The value of m is estimated by the least-square fitting of the overlapping area of the original and shifted spatial frequency distribution. The value of ϕ_0 is obtained when $k_x = k_m$ and $k_n = \Delta\phi$ according to Equ. 4. At last, a Tukey window ($\alpha = 0.25$) is multiplied on the extended $\tilde{R}(k_x)$ to round off the sharp edge and eliminate the high frequency artifacts. The final SIOCT image is then re-transformed into spatial space using the extended spatial frequency distribution $\tilde{R}(k_x)$.

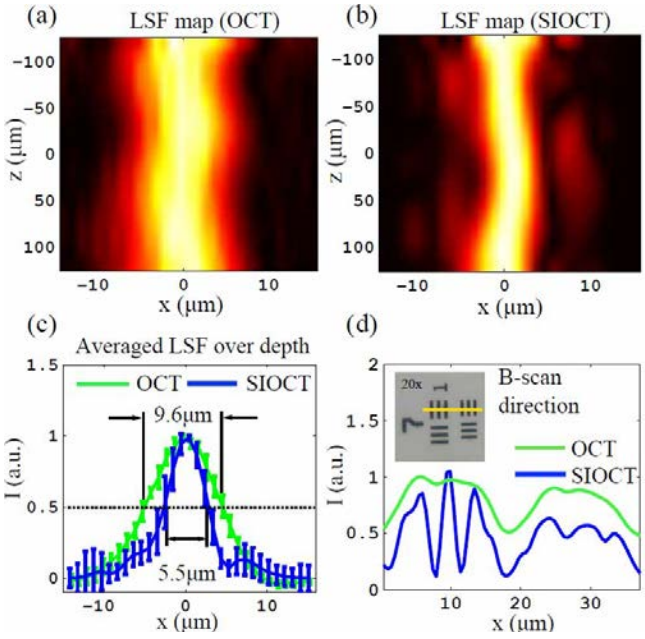

Fig. 2. (a-b) Line spread function (LSF) map through a depth of focus of $\sim 200\mu m$ in OCT and SIOCT. The curvy pattern is caused by slight asymmetry from experiments. (c) Averaged LSF $\pm SD$ over the depth of focus from (a-b). (d) B-scan intensity on the surface of the target by OCT and SIOCT. Inset: 20x microscopic image of the AF-1951 target. The yellow line depicts the B-scan location.

To characterize the resolution of SIOCT, we firstly imaged the edge of a large element (Group 2: element 1) on a AF-1951 resolution target. The derivative of the B-scan intensity from the edge is calculated as the line spread function (LSF). Figure 2(a-b) illustrate the LSF measurements throughout the depth of focus in conventional OCT and SIOCT by vertically translating the sample. The target was shifted at various depths around the focal point and the smooth map along z is obtained by an interpolation. The actual measurements were per-

formed at the depth of -112, -72, -28, 28, 64, 120 μm with respect to the focus spot. Each measured LSF is normalized to have the maximum value equal to 1. The averaged LSF over depth are compared in Fig. 2(c). The diffraction limited transverse resolution is measured to be $\sim 9.6\mu m$ while $\sim 5.5\mu m$ in SIOCT. The enhancement of the resolution is demonstrated in Fig. 2d. Each three strips of two small elements (Group 7: element 1 and 2) are clearly resolved by SIOCT in contrast to conventional OCT.

To further demonstrate the resolution enhancement, we composed a phantom with $0.8\mu m$ diameter polystyrene microspheres. The sphere solution was dispersed in a hot Agarose gel solution which forms a clear solid phantom when cooling down. Figure 3(a-b) shows the comparison of the B-scan images from conventional OCT and SIOCT. The mean intensity along depth from three regions are compared in Fig. 3c, which evidenced the resolution improvement over $370\mu m$ depth span.

To demonstrate the SIOCT on a biological sample, we also imaged chicken adipose tissue with OCT and SIOCT shown in Fig. 3(d-e), and the enhancement of the lateral resolution is visually significant as well. Note that we increased the scanning range from 0.25mm (Fig. 3a,b) to 1mm (Fig. 3d,e) with A-line interval from $1\mu m$ to $4\mu m$, the sampling rate drops to about 3 points per modulation period and the resolution improvement is still appreciable. Yet with less precision of estimating the phase, the SIOCT image is subject to more noise.

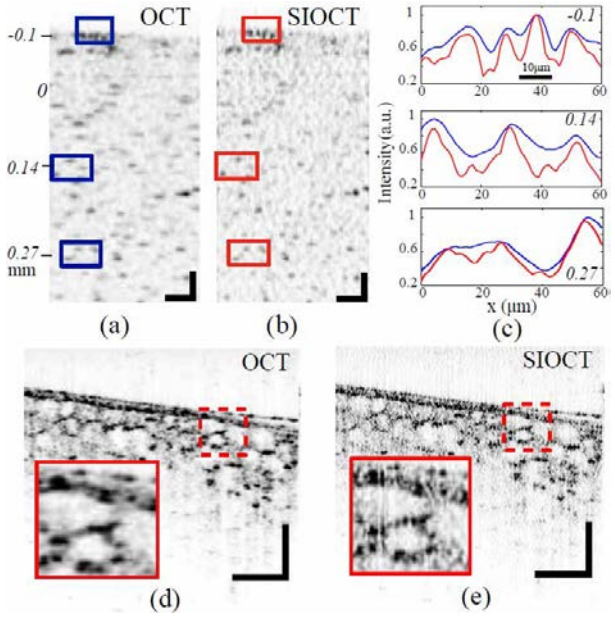

Fig. 3. (a-b) B-scan image of $1\mu m$ microspheres phantom with OCT and SIOCT. Bar = $50\mu m$. The label on the depth is relative to the focal spot. (c) The mean intensity over z from the squared areas in (a-b). Blue=OCT; Red=SIOCT. (d-e) B-scan image of chicken adipose tissue with OCT and SIOCT. Bar = $200\mu m$. Insets in figures are expanded from the dashed regions for a clearer view.

Without modifying the illumination beam profile, the SIOCT enhances the resolution by a factor of two. The sacrifice is that multiple B-scan frames of at the same location are required to numerically synthesize the extended spatial frequency distribution. In principle only three frames with 120° phase increment are needed. With a current state-of-the-art high speed OCT system, the A-line rate is over 400MHz which can make multi-frame collection at the level of 1 ms. Assuming $10\mu m$ drifting, the tolerant motion speed is around 10 mm/s which can be well satisfied [12]. Therefore, SIOCT can be adapted in real-time imaging and an electro-optic or acousto-optic modulators can be used for high speed modulation.

The maximum limit of the temporal modulation frequency is reached when the spatial pattern period is the system resolution. The precise transform from temporal to spatial pattern is to convolute the sinusoidal wave with the point spread function. Thus when the modulation frequency exceeds the resolution limit, such a transform is no longer able to produce a spatially varying pattern. This technique can be combined with other resolution enhancement methods mentioned in the introduction to improve the resolution further.

We acknowledge our financial support from NIH grant R01CA128641, R01EB003682 and NSF grant CBET-0937987 to VB, NIH grants R01EY019951, RC4EF021357 and NSF grant CBET-1055379 to HFZ.

References

1. D. Huang, E. A. Swanson, C. P. Lin, J. S. Schuman, W. G. Stinson, W. Chang, M. R. Hee, T. Flotte, K. Gregory, C. A. Puliafito, and J. G. Fujimoto, Science **254**, 1178 (1991).
2. M. Wojtkowski, R. Leitgeb, A. Kowalczyk, T. Bajraszewski, and A. F. Fercher, Journal of Biomedical Optics **7**, 457 (2002).
3. L. Yu, B. Rao, J. Zhang, J. Su, Q. Wang, S. Guo, and Z. Chen, Opt. Express **15**, 7634 (2007).
4. T. S. Ralston, D. L. Marks, P. S. Carney, and S. A. Boppart, Nat Phys **3**, 129 (2007).
5. Z. Ding, H. Ren, Y. Zhao, J. S. Nelson, and Z. Chen, Opt. Lett. **27**, 243 (2002).
6. C. Blatter, B. Grajciar, C. M. Eigenwillig, W. Wieser, B. R. Biedermann, R. Huber, and R. A. Leitgeb, Opt. Express **19**, 12141 (2011).
7. R. A. Leitgeb, M. Villiger, A. H. Bachmann, L. Steinmann, and T. Lasser, Opt. Lett. **31**, 2450 (2006).
8. L. Liu, C. Liu, W. C. Howe, C. J. R. Sheppard, and N. Chen, Opt. Lett. **32**, 2375 (2007).
9. L. Liu, J. A. Gardecki, S. K. Nadkarni, J. D. Toussaint, Y. Yagi, B. E. Bouma, and G. J. Tearney, Nat Med **17**, 1010 (2011).
10. M. G. L. Gustafsson, Journal of Microscopy **198**, 82 (2000).
11. J. Lu, W. Min, J.-A. Conchello, X. S. Xie, and J. W. Lichtman, Nano Letters **9**, 3883 (2009).
12. R. K. Wang, Applied Physics Letters **90**, 054103 (2007).

Informational Fourth Page

In this section, please provide full versions of citations to assist reviewers and editors (OL publishes a short form of citations) or any other information that would aid the peer-review process.

References

1. D. Huang, E. A. Swanson, C. P. Lin, J. S. Schuman, W. G. Stinson, W. Chang, M. R. Hee, T. Flotte, K. Gregory, C. A. Puliafito, and J. G. Fujimoto, "Optical coherence tomography," Science **254**, 1178–1181 (1991).
2. M. Wojtkowski, R. Leitgeb, A. Kowalczyk, T. Bajraszewski, and A. F. Fercher, "In vivo human retinal imaging by fourier domain optical coherence tomography," Journal of Biomedical Optics **7**, 457–463 (2002).
3. L. Yu, B. Rao, J. Zhang, J. Su, Q. Wang, S. Guo, and Z. Chen, "Improved lateral resolution in optical coherence tomography by digital focusing using two-dimensional numerical diffraction method," Opt. Express **15**, 7634–7641 (2007).
4. T. S. Ralston, D. L. Marks, P. S. Carney, and S. A. Boppart, "Interferometric synthetic aperture microscopy," Nat Phys **3**, 129 – 134 (2007).
5. Z. Ding, H. Ren, Y. Zhao, J. S. Nelson, and Z. Chen, "High-resolution optical coherence tomography over a large depth range with an axicon lens," Opt. Lett. **27**, 243–245 (2002).
6. C. Blatter, B. Grajciar, C. M. Eigenwillig, W. Wieser, B. R. Biedermann, R. Huber, and R. A. Leitgeb, "Extended focus high-speed swept source oct with self-reconstructive illumination," Opt. Express **19**, 12141–12155 (2011).
7. R. A. Leitgeb, M. Villiger, A. H. Bachmann, L. Steinmann, and T. Lasser, "Extended focus depth for fourier domain optical coherence microscopy," Opt. Lett. **31**, 2450–2452 (2006).
8. L. Liu, C. Liu, W. C. Howe, C. J. R. Sheppard, and N. Chen, "Binary-phase spatial filter for real-time swept-source optical coherence microscopy," Opt. Lett. **32**, 2375–2377 (2007).
9. L. Liu, J. A. Gardecki, S. K. Nadkarni, J. D. Toussaint, Y. Yagi, B. E. Bouma, and G. J. Tearney, "Imaging the subcellular structure of human coronary atherosclerosis using micro-optical coherence tomography," Nat Med **17**, 1010–1014 (2011).
10. M. G. L. Gustafsson, "Surpassing the lateral resolution limit by a factor of two using structured illumination microscopy," Journal of Microscopy **198**, 82–87 (2000).
11. J. Lu, W. Min, J.-A. Conchello, X. S. Xie, and J. W. Lichtman, "Super-resolution laser scanning microscopy through spatiotemporal modulation," Nano Letters **9**, 3883–3889 (2009).
12. R. K. Wang, Applied Physics Letters **90**, 054103 (2007).